Faraday Discussions

COMMUNICATION

Smart Supramolecular Sensing with Cucurbit[*n*]urils: Probing Hydrogen Bonding with SERS

Received 00th April 2017,
Accepted 00th April 2017

DOI: 10.1039/x0xx00000x

www.rsc.org/

B. de Nijs,[a†] M. Kamp,[b] I. Szabó,[c] S. J. Barrow,[b] F. Benz,[a] G. Wu,[b] C. Carnegie,[a] R. Chikkaraddy,[a] W. Wang,[a] W. M. Deacon,[a] E. Rosta,[c] J. J. Baumberg[a] and O. A. Scherman[b†]

Rigid gap nano-aggregates of Au nanoparticles formed using cucurbit[*n*]uril (CB[*n*]) molecules are used to investigate competitive binding of ethanol and methanol in an aqueous environment. We show it is possible to detect as little as 0.1% methanol in water and a ten times higher affinity to methanol over ethanol, making this a useful technology for quality control in alcohol production. We demonstrate strong interaction effects in the SERS peaks, which we demonstrate are likely from hydrogen bonding of water complexes in the vicinity of the CB[*n*]s.

Surface-Enhanced Raman Scattering (SERS) has attracted wide-spread interest on account of its potential for sensing down to the single molecule level[1-8]. This has led to a wealth of research on detecting trace amounts of pollutants[9], poisons[10] and explosives[11,12], achieved by plasmonic constructs such as core-shell nanoparticles[13], nanostars[14-18], nanoparticle aggregates[19,20], nanowire junctions[21-24] and plasmonic tips[25-27] (tip-enhanced Raman Scattering, TERS). Recently, SERS has also been used to study reactions[28] and conformational changes in molecules[29]. Only few studies have been performed where SERS is exploited to study solvent molecules as analytes[30,31], and usually only their bulk Raman signal is mentioned[32].

Cucurbit[*n*]urils or CB[*n*]s are a family of macrocyclic molecules that have attracted increased attention on account of their excellent molecular recognition properties and high binding affinities for guest molecules[33]. The ability of CB[*n*] to act as a sub-nm molecular spacer to induce and control the aggregation of gold nanoparticles (AuNPs) and to subsequently bind analyte molecules at room temperature within their hydrophobic cavities is a major area of research. These simple, robust CB[*n*]-AuNP constructs have proven particularly interesting in the area of molecular sensing[34]. Using SERS, it is possible to detect a wide variety of analytes which form 1:1 complexes within CB[7][35]. This host-guest chemistry is also capable of performing quantitative multiplexing of neurotransmitters in biological media such as urine[36]. Moreover, on account of the strong field confinement (>x100) within the cavities between the gold nanoparticles, analyte concentrations down to the nanomolar regime can be detected[36]. Plasmonic coupling at such short distances is highly sensitive to variations in the cavity properties, making it possible to resolve thickness differences of 0.1 nm and observe refractive index changes from molecular filling[37].

Here, we shift our attention to the detection of solvent molecules and show that CB[*n*]-AuNP constructs can be used to detect the presence of methanol (MeOH) in ethanol (EtOH)/water mixtures. In addition to being useful in view of public health and safety, our results show that the hydrogen bonding between MeOH and water and EtOH and water can be directly probed using plasmonic CB[*n*]-AuNP constructs, opening up avenues to study molecular dynamics of solvent molecule mixtures using SERS. With DFT calculations we explore the binding behaviour of MeOH, EtOH to CB[5] and CB[6] further and show that in addition to host-guest complexation, the direct aqueous environment is probed as well using such experimental techniques.

[a] NanoPhotonics Centre, Cavendish Laboratory, University of Cambridge, Cambridge CB3 0HE, UK
[b] University of Cambridge, Melville Laboratory for Polymer Synthesis, Department of Chemistry, Cambridge CB2 1EW, UK.
[c] King's College London, Department of Chemistry, London, UK.
† Correspondence should be addressed to bd355@cam.ac.uk or oas23@cam.ac.uk.
Electronic Supplementary Information (ESI) available: Additional experimental results, additional computational details and results, supplementary references. See DOI: 10.1039/x0xx00000x

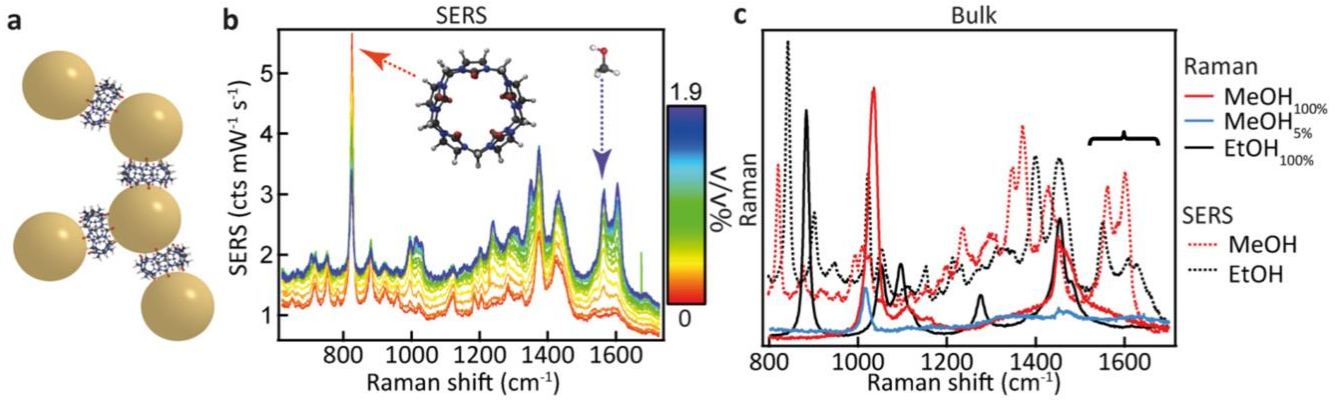

Figure 1: SERS-based MeOH sensing in an aqueous environment. **a**) Cucurbit[*n*]uril-gold nanoparticle construct with a 0.9 nm inter-particle spacing. **b**) SERS spectra of CB[5]-AuNP constructs showing spectral changes upon adding up to 1.9 v/v% MeOH, resulting in strong peaks in the region from 1520 cm^{-1} to 1640 cm^{-1} (dashed arrow). **c**) Bulk measurements of MeOH, MeOH in water, and EtOH showing no peaks at 1564 cm^{-1} and 1604 cm^{-1}.

Experimental details

Citrate-stabilized gold nanoparticles (60 nm) were purchased from BBI Solutions, and used as received (which have previously shown to be effective). Ethanol (EtOH, absolute, > 99.8%) and methanol (MeOH, reagent grade) were obtained from Fisher Scientific and used as received. CB[5] and CB[6] were separated from a CB[*n*] mixture synthesised in house using previously published procedures[38]. A CB[5] solution in water [1 mM] was bubbled with nitrogen for 30 min. CB[6] is only soluble to a maximum of 200 mM[39], therefore a 1 g/L suspension was prepared and bubbled with nitrogen before diluting it by a factor 50 with AuNP dispersions as described below.

Sample mixtures were prepared by mixing CB[*n*] solution, AuNP dispersion, and MeOH/EtOH water mixtures. Typically, 20 µL of the CB[*n*] solution was placed in a plastic cuvette and then 980 µL gold NP dispersion added to the CB[*n*] using an Eppendorf pipette, by which the CB[*n*] and the AuNPs are mixed. After waiting 4 min to allow for the formation of gold NP aggregates through bridging by the CB[*n*], 20 µL of an EtOH/MeOH mixture was added and mixed in using a 1 mL pipette. Alternatively, to carry out a concentration series measurement, amounts of 1 µL of MeOH were added to the CB[*n*]-AuNP constructs repeatedly using a 10 µL pipette.

SERS measurements were carried out using a Renishaw inVia Raman microscope equipped with a Plan 5x objective with a numerical aperture of 0.12. An excitation wavelength of 785 nm was chosen in order to excite chain plasmons in the gold NP aggregates[40,41]. The laser beam entered the sample from the (open) top of the cuvette. By performing a depth series, the optimum distance of the solution to the laser, which is the location yielding maximum number of counts, was determined. At the ideal distance the focal point of the laser is near the liquid-air interface. This results in neither the illumination path nor the collection path passing through or near the plastic of the cuvette. The spectrum from the cuvette material is known (see Supporting Information) and no contribution from the cuvette is seen in the recorded data. Each SERS measurement was performed with an integration time of 10 s for 3 accumulations at full laser power (130 mW over the large solution volume). Spectra were recorded in the range of 620 cm^{-1} – 1730 cm^{-1} with a resolution of 1.1 cm^{-1}.

Table 1. Structural Parameters for uncomplexed CB[5]-CB[8]

	CB[5][a]	CB[6][a]	CB[7][a]	CB[8][a]
portal diameter (Å)	2.4	3.9	5.4	6.9
cavity diameter (Å)	4.4	5.8	7.3	8.8
cavity volume ($Å^3$)	82	164	279	479
outer diameter (Å)	13.1	14.4	16.0	17.5
height (Å)	9.1	9.1	9.1	9.1

[a]*adapted with permission from [42]. ©2000 ACS.*

Results

CB[5] has a hydrophobic cavity with an internal diameter of 4.4 Å (see Table 1). MeOH[43] has a diameter of 2.1 Å and a kinetic diameter of 3.6 Å, hence the macromolecular CB[5] spacer could potentially sequester or sieve out single MeOH molecules from solution, placing them inside the plasmonic hotspots. Upon adding increasing amounts of MeOH (0 - 1.9 v/v%) to CB[5]-AuNP constructs in water, clear spectral changes emerge with distinct peaks at 1564 cm^{-1} and 1604 cm^{-1} (Figure 1b,c: green). Interestingly, these peaks do not correspond to bulk Raman spectra (Figure 1c) measured for MeOH (black) or EtOH (red). The peaks also do not correspond to a 10% MeOH water mixture (blue trace), which displays a drastically decreased Raman signal and a slightly blue-shifted peak at 1030 cm^{-1}.

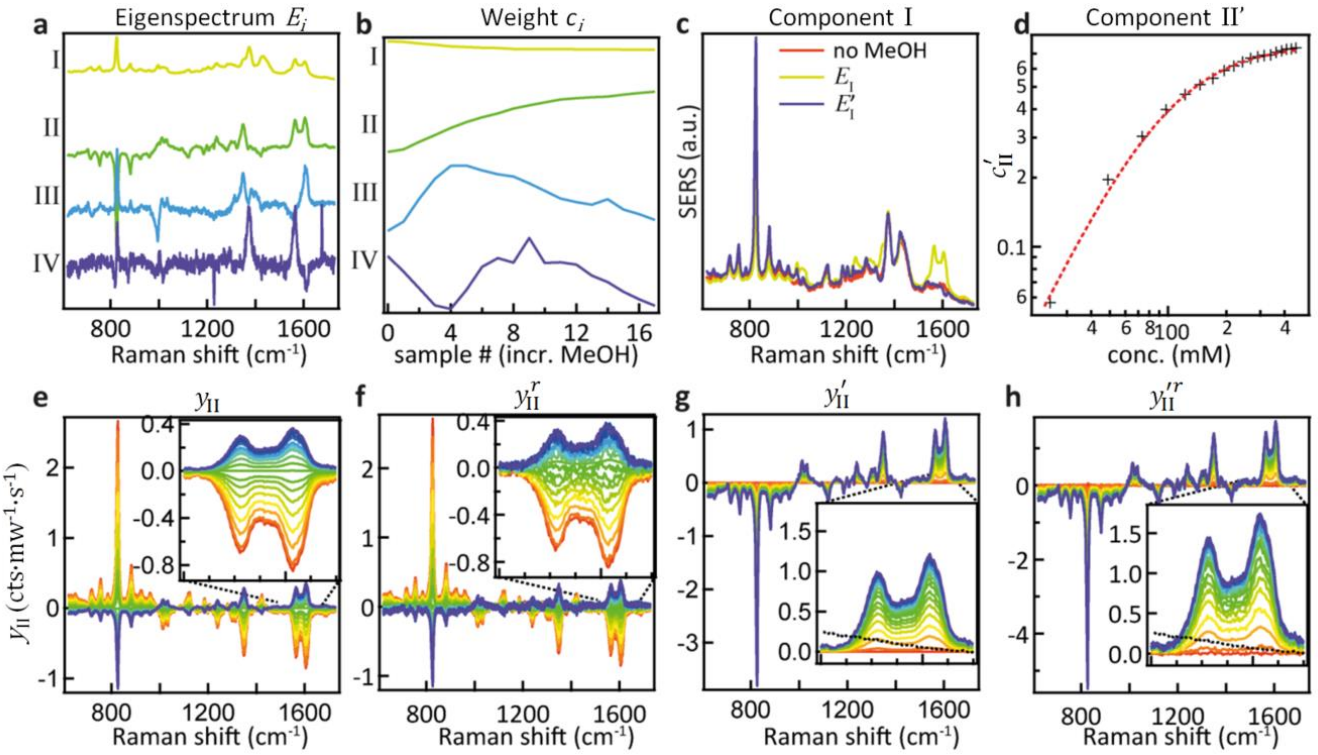

Figure 2: Principal component analysis of spectral changes in CB[5]-AuNP aggregates upon addition of MeOH. **a**) The first four component eigenspectra E_i. **b**) Weights c_i for each of the components showing their variation upon addition of MeOH from 0-500mM. **c**) Comparison of E_{I}, E_{I}' and a pure CB[5] spectrum without MeOH. **d**) The modified PCA II weight c_{II}' plotted against MeOH concentration shows clear correlation. **e**) Plot showing E_{II} multiplied by its weight highlighting the changes upon addition of MeOH. **f**) Reconstituted change in PCA II, plotted by subtracting $y_{\mathrm{I,III-VI}}$ from the raw dataset. **g**,**h**) Same plots as **e**,**f** but with the weight offset by its value at m=0 v/v% MeOH, showing the reconstructed spectral changes for PCA II. The dotted line in the inset is the bulk Raman signal of MeOH in this region.

The differences in signal strength and peak location demonstrate that the obtained spectra in Figure 1b are SERS signals. A second notable change is the decrease in the 830 cm^{-1} peak, a characteristic peak of CB[*n*] SERS spectra, showing that the new peaks arise from some form of interaction with the CB[5]-AuNP constructs. Generally, quantifying such effects has proven difficult as SERS spectra suffer from inherent background fluctuations, preventing simple comparisons among peak intensities. In addition, the decrease in peak intensity of the CB[*n*] with the addition of the analyte (here MeOH) shows that the CB[5] peak cannot always be used as an internal standard even though the CB[5] concentration is kept nearly constant throughout the experiments. These issues render SERS, without supplementation, inadequate as a quantitative analytical technique.

Here we demonstrate that by using principal component analysis (PCA) we can accurately identify and quantify the individual analyte components and correlate SERS intensities with analyte concentrations to extract new information. PCA expresses data into a new basis set of mathematically orthogonal *components* in order of decreasing variability, with the aim of detecting trends in noisy, variable data such as SERS spectra. This is particularly useful when we scan the concentration m of one analyte. In the case of this series of spectra, each component consists of an '*eigenspectrum*' $E_i(\nu)$ (a set of spectral components which change together) and a *weight* c_i (often known as a PCA 'score') which gives the contribution of its associated eigenspectrum to the measured spectrum. The contribution y_i of a single component to the full spectrum at concentration m is then

$$y_i(m) = c_i(m)\, E_i \qquad \text{eq. 1}$$

Combining all contributions yields the counts at each wavelength, reconstructing the measured spectrum

$$y_{\mathrm{tot}}(\nu) = \sum_{i=\mathrm{I}}^{N} c_i\, E_i(\nu) \qquad \text{eq. 2}$$

where y_{tot} is the SERS emission at wavenumber ν. A practicality regarding PCA is that the physical meaning of the *eigenspectra* can only be attributed with additional knowledge of the experimental system.

PCA is used to exploit the change in spectra upon analyte addition to isolate the SERS contributions of the individual components from a concentration series (see Figure 2a). The *eigenspectrum* of the first component obtained using PCA (E_{I}) closely resembles the characteristic CB[5] SERS and bulk Raman spectra, see Figure S1. The *eigenspectrum* of the second major component (E_{II}) is attributed to MeOH since a steady

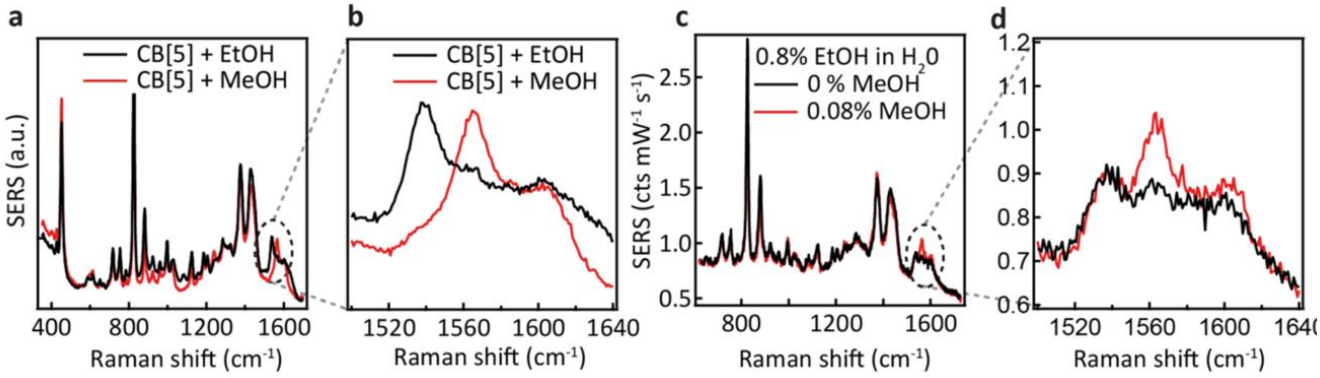

Figure 3: CB[5]-AuNP SERS demonstrating MeOH and EtOH detection. **a**) SERS spectra of EtOH (red) and MeOH (black). **b**) Spectral region of interest showing distinct differences in the peak position for EtOH (1540 cm^{-1}) and MeOH (1564 cm^{-1}). **c**) Detection of 4 v/v% MeOH (black) or absent (red), when combined with mixture of 40 v/v% EtOH:water. **d**) Highlighted region shows clear peak at 1564 cm^{-1}.

increase in its corresponding weight is observed with the addition of analyte (Figure 2b-d).

However, E_{II} does not only contain MeOH lines, but also shows a reduction (negative peaks) in CB lines (Figure 2a,II). This clearly shows the existence of some chemical interaction between the components. As a result of the basic properties of PCA since variability is expressed as a weight about the origin of the principle axes, $c_{\mathrm{II}}(0)$ has a negative value at 0% MeOH, and E_{I} (light blue trace in Figure 2c) does not represent a clean CB[5] spectrum. This contribution can be removed from E_{I} by extracting the fraction of E_{II} from E_{I} at 0% MeOH using

$$E'_{\mathrm{I}} = E_{\mathrm{I}} - E_{II} \times \frac{c_{\mathrm{II}}(0\%)}{c_{\mathrm{I}}(0\%)} \qquad \text{eq. 3}$$

This essentially moves the data set along the PC axis II, making the lowest weight value [corresponding to no MeOH added] equal to 0. This results in E'_{I} (dark blue in Figure 2c) closely matching the CB[5] spectrum ('no MeOH', red) without E_{II}. Similarly we define

$$c'_{\mathrm{II}}(m) = c_{\mathrm{II}}(m) - c_{\mathrm{I}}(m) \times \frac{c_{\mathrm{II}}(0\%)}{c_{\mathrm{I}}(0\%)} \qquad \text{eq. 4}$$

now resulting in only positive weight values for the modified second component. Plotting this c'_{II} versus the added analyte concentration gives a clear saturation curve (Figure 2d) which is well fit by the Hill-Langmuir equation,

$$c'_{\mathrm{II}} = A_{\mathrm{II}}[1 + (K_D/[\mathrm{MeOH}])^n]^{-1} \qquad \text{eq. 5}$$

where K_D is the dissociation constant (here 140 mM), n=2.0 is the Hill coefficient which is here markedly higher than 1 indicating a cooperative binding mechanism for the MeOH, and the maximum $A_{\mathrm{II}} = 0.73$ is the saturated component value.

The components extracted using PCA can be exploited to visualise, without noise present, the spectral changes happening as MeOH is added (Figure 2e). The effect of dimensionality reduction (with only 6 components being significant and taken into account) can be observed by taking the dataset and subtracting the contributions from all components (I-VI) except II:

$$y^r_{\mathrm{II}}(m) \simeq y_{\mathrm{tot}}(m) - \sum_{i=\mathrm{I},i\neq\mathrm{II}}^{\mathrm{VI}} c_i(m)\, E_i \qquad \text{eq. 6}$$

reconstituting the contribution of the second component (Figure 2f). The good match between y_{II} and y^r_{II} in Figures 2e,f show that individual spectra can indeed be suitably reconstructed from these components, even when interacting.

The effect of shifting the data origin to match m=0 can be seen from using the modified c'_{II} and E'_{I}, with $y'_i = c'_i E'_i$ and the equivalent of eqn.6 to calculate y'^r_{II}. This gives the induced changes on adding MeOH concentrations up to 2% (Figure 2g,h) and confirms that plotting the reconstituted eigenspectra yields spectral changes characteristic for the added analyte.

These more complex spectral changes with increasing analyte concentration clearly show that the SERS peaks are correlated with MeOH concentration, even though the isolated spectral change (Figure 2h) shows minimal resemblance to the bulk MeOH Raman spectrum (black dashed). This radical difference between the bulk (Raman) and SERS spectra of MeOH suggests that binding effects or other strong molecular interactions between the MeOH and either the gold, the CB[5], or other moieties in the system play an important role in the detection. We thus explored this interaction further.

Comparing EtOH with MeOH as analyte, similar peaks are observed throughout the SERS spectra (Figure 3a) but with a distinct exception in the region around 1550 cm^{-1} (Figure 3b). While a similar doublet of peaks is observed here for both EtOH and MeOH with one peak

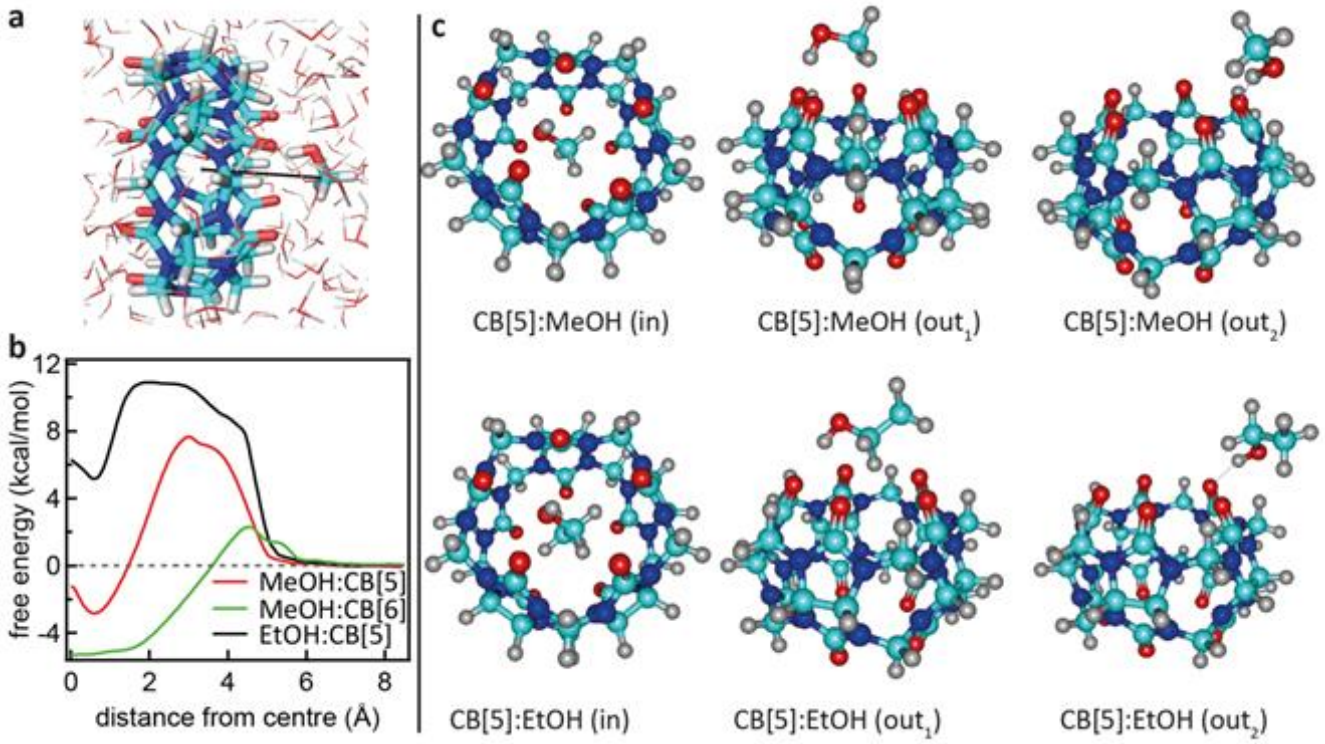

Figure 4: Calculated interaction between CB[5] and MeOH or EtOH. **a**) Rendering showing the MeOH being moved into the CB[5] cavity in aqueous environment. **b**) Free energy profiles for MeOH and EtOH ligands passing through the carbonyl portals of CB[5] and CB[6] and into the molecular cage. **c**) Renderings of geometry-optimized alternative complexations between CB[5] and MeOH or EtOH (see also the computational details in Supplementary Information).

located at 1604 cm^{-1}, for EtOH a shifted peak at 1539 cm^{-1} is observed compared to the MeOH at 1564 cm^{-1}. The similarity between these spectra suggests similar but non-identical interactions between the CB[5] and these analytes.

We now explore the capability to combine EtOH and MeOH SERS detection, which is crucial for application to consumer-alcohol contamination. We also investigate a hypothesis that the interaction behaviour originates from size-specific encapsulation of methanol inside CB[5]. Two mixtures (20 µL) are added as analyte to the CB[5]-AuNP sensing aggregates (980 µL), both containing 40 v/v% EtOH in water, which in one case is further spiked with 4 v/v% MeOH. For the non-spiked sample, a weaker version of the two ethanol peaks is observed (Figure 3c,d). For the spiked sample, an additional sharp peak at 1564 cm^{-1} is seen along with a small increase in the 1604 cm^{-1} peak, which corresponds to the MeOH SERS spectrum previously determined. Notice that the final concentration of EtOH in the 1 mL measurement volume is 0.8 v/v%, and that we are able to measure a final concentration as low as 0.08 v/v%. Whilst the total added amount of MeOH is 10 times lower than the amount of EtOH added, a comparably intense SERS peak is observed (~0.1 cts $mW^{-1}s^{-1}$ each). This suggests a preferential interaction between MeOH-CB[5] over EtOH-CB[5].

To support this, we calculated the association energies using quantum chemical calculations at the DFT B3LYP-Def2-TZVP-D3 level (See SI4 Table S1) as well as biased Umbrella Sampling MD free energy calculations (Figure 4a,b). Since there is a 2.9 kcal mol^{-1} free energy gain for the MeOH to reside in the CB[5] cavity based on the MD simulations and 0.7 or 2.4 kcal mol^{-1} based on the DFT calculations using SMD or PCM solvent models, respectively, inclusion should be favourable. We also calculated that the MeOH/EtOH molecules have to overcome a 7.7 kcal mol^{-1} free energy barrier to pass through the carbonyl portals into the CB[5] or CB[6] cavities along the trajectory marked (Figure 4a). This kinetic barrier is in line with observed inclusion results for methane in CB[5] where heating to 80°C is required for sequestration to occur[44]. Nevertheless, our experiments clearly point at a preferential molecular interaction for MeOH-CB[5] with respect to EtOH-CB[5]. To explore the possibility that the outside of CB[5] preferentially interacts with MeOH over EtOH, we calculated the association free energy for the CB[5] complexed with MeOH and EtOH more comprehensively (Table S1). Only a marginally lower free energy is found for the MeOH, which is not enough to explain the observed preferential interaction. Since the calculations indicate that inclusion of EtOH by CB[5] is highly unfavourable, these experiments suggest that in such

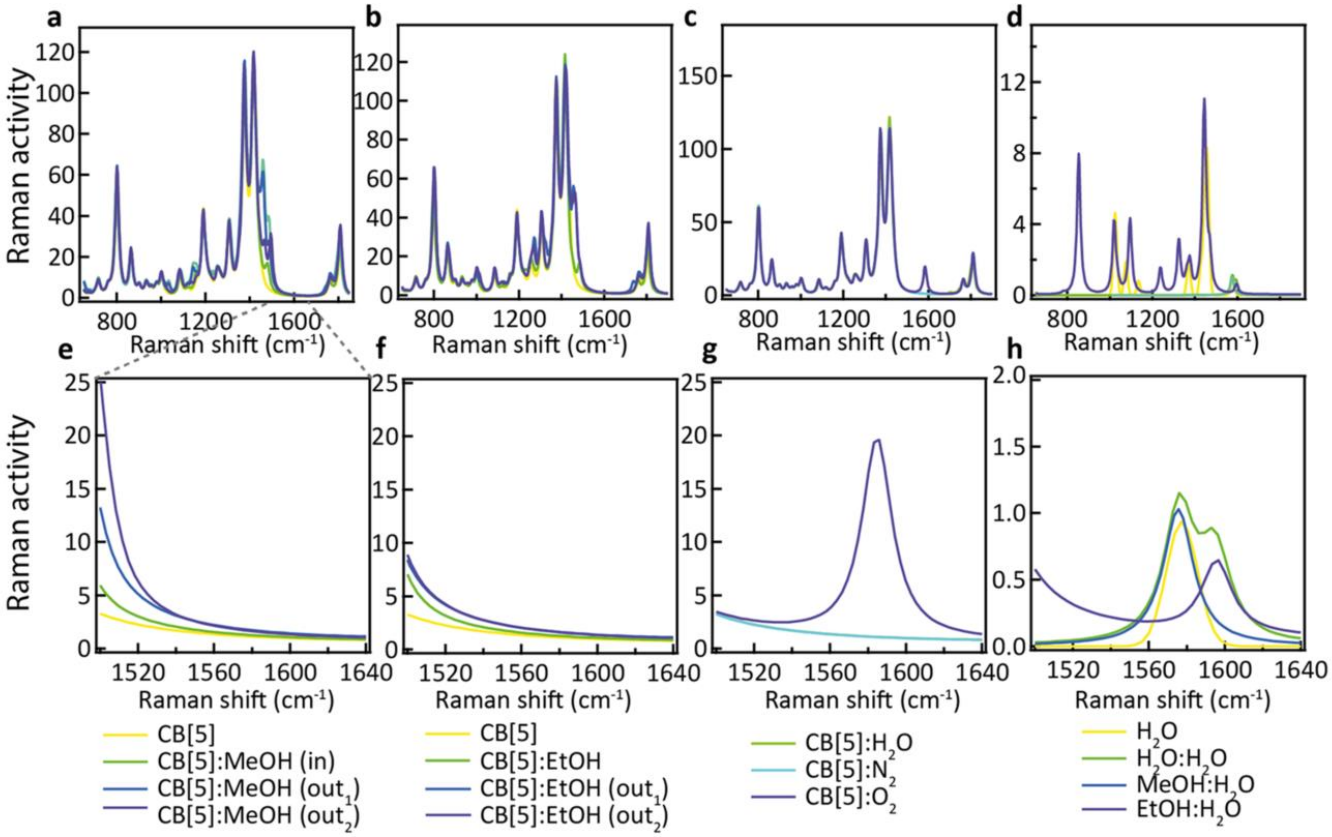

Figure 5: Calculated vibrational spectra for plausible molecular binding geometries with CB[5] present in the probed system. Positioned in and around the macro molecular structure: **a**) MeOH, **b**) EtOH, **c**) water, nitrogen, and oxygen. **d**) Water molecules hydrogen-bound with water, MeOH, EtOH, without CB[5]. **e**-**h**) Highlighted range of interest showing that only oxygen and hydrogen-bound water have peaks at these wavenumbers.

systems the outside of the CB[5] is probed as well since EtOH is still readily detected. Interestingly, the fitted dissociation constant (K_D) for EtOH-CB[5] is lower than the K_D fitted for MeOH-CB[5] (SI: Table S2).

It has been shown in literature that MeOH inclusion by CB[5] does occur in the presence of ammonia.[45] Ammonia is absent in the current experiments, but sodium, a citrate counter-ion, has a similar interaction with the portals[46] and is present in the system. It is clear that subtle solvent effects influence this binding behaviour as bubbling nitrogen through the CB[*n*] solution, or between different batches of CB[5] (not shown here), results in different but consistent spectral changes, demonstrating a strong interaction of the analyte with its environment.

What is not yet explained are the positions of the SERS peaks that do not match any of the bulk Raman signals. This shows again that the analyte interacts with either the CB[*n*] or other chemical moieties in its direct environment. To identify the potential nature of these SERS peaks, vibrational spectra were calculated for each of the CB[5]:MeOH and CB[5]:EtOH binding geometries presented in Figure 4, and for other complexes of CB[5] with competitive guests potentially present in the ambient system (H_2O, N_2, O_2). These are compared to vibrational spectra of hydrogen-bonded complexes (denoted by a colon) of MeOH and EtOH with water. All three configurations of CB[5]:MeOH and CB[5]:EtOH show additional peaks only in the region of 1450 cm^{-1} to 1500 cm^{-1} (Figure 5a,b,e,f) but no peaks near those observed at 1539 cm^{-1}, 1564 cm^{-1}, or 1604 cm^{-1}. While no clear change in this 1500 - 1620 cm^{-1} band is observed for nitrogen or water inside CB[5], placing oxygen in the molecular cavity predicts a clear line at 1585 cm^{-1} (Figure 5c,g) directly from the oxygen molecule, which is thus one possibility.

However even without CB[5] present, calculated vibrational spectra for hydrogen-bonded complexes between MeOH and water (MeOH:H_2O), between EtOH and water (EtOH:H_2O), and between two water molecules (H_2O:H_2O) also exhibit peaks in the same region (Figure 5d,h). These are at 1576 cm^{-1} for water/H_2O:H_2O/MeOH:H_2O, are at 1593 cm^{-1} for H_2O:H_2O, and at 1597 cm^{-1} for EtOH:H_2O. Since it is unlikely that the oxygen concentration increases when MeOH is added (although this cannot be excluded), this suggests it is the hydrogen bonding between the analyte and water in or near the CB[5] cavity that is probed by SERS. Strong or arrested hydrogen bonding is expected as otherwise broader peaks would be observed, hinting

at a local 'solid' phase with temporarily arrested dynamics.

Using CB[6] instead of CB[5] results in peak positions at 1539 cm^{-1} and 1604 cm^{-1} (see SI Figure S2), matching the dominant peaks obtained with EtOH and CB[5], further supporting the idea that the peaks are a result of hydrogen bonding. The exact configuration of the MeOH:H_2O and EtOH:H_2O complexation is not yet clear, nor the observed influence of the direct environment, but the use presented here of CB[*n*]-AuNP constructs in combination with MeOH and EtOH appears to be a powerful method in probing the behaviour of water in confined spaces. Considering the immense sensitivity achievable with SERS (down to single molecules) these advances open up new avenues to probe molecular mechanics and solvent-solvent interactions with an unprecedented level of detail. We also demonstrate that such a system can be practically used for the detection of MeOH in alcoholic liquids providing a low-cost potential means of screening for health risks in consumer products.

Conclusions

Using CB[5] and CB[6]-based self-assembly of gold nanoparticles into sensing aggregates, we demonstrated SERS-based detection of as little as 0.1 v/v% of methanol in water. We also demonstrated that even in ethanol/water mixtures, 4 v/v% methanol (the upper safe consumption limit) can be distinctly detected. We show that principal component analysis can be used to isolate the methanol contribution to the SERS spectra. Our data imply that CB[*n*] molecules either sequester or strongly interact with MeOH and to a lesser extent EtOH, and the obtained signals arise from interactions with water around the molecular spacers. We conclude that this provides a powerful test bed for probing molecular dynamics at the nanoscale.

Acknowledgements

We acknowledge financial support from the UK's Engineering and Physical Sciences Research Council (grants EP/L027151/1, EP/K028510/1, EP/L015978/1, EP/N020669/1) and the European Research Council (grants LINASS 320503, MSCA-IF-2015-EF SPARCLEs 7020005 and MSCA-IF-2014-EF NANOSPHERE, 658360). RC acknowledges support from the Dr. Manmohan Singh scholarship from St. John's College. FB acknowledges support from the Winton Programme for the Physics of Sustainability. CC acknowledges support from the UK National Physical Laboratories. GW thanks the Leverhulme Trust (Natural material innovation for sustainable living) for the support.

Notes and references

1 S. Nie and S. R. Emory. *Science*, 1997, **275**, 1102.
2 N. P. W. Pieczonka and R. F. Aroca, *Chem Soc Rev*, 2008, **37**, 946.
3 C. J. L. Constantino, T. Lemma, P. A. Antunes and R. F. Aroca. *Anal Chem*, 2001, **73**, 3674.
4 Q. Si. *Phys Rev Lett, 1997,* **78**, 1667.
5 J. N. Anker, W. P. Hall, O. Lyandres, N. C. Shah, J. Zhao and R. P. Van Duyne. *Nat Mater*, 2008, **7**, 442.
6 S. Lal, S. Link and N. J. Halas. *Nat Photonics*, 2007, **1**, 641.
7 M. D. Sonntag, J. M. Klingsporn, A. B. Zrimsek, B. Sharma, L. K. Ruvuna and R. P. Van Duyne. *Chem Soc Rev*, 2014, **43**, 1230.
8 K. Kneipp, H. Kneipp, I. Itzkan, R. R. Dasari and M. S. Feld. *J Phys: Cond Mat*, 2002, **14**, R597.
9 J. Ofner et al. *Anal Chem*, 2016, **88**, 9766.
10 M. Mulvihill, A. Tao, K. Benjauthrit, J. Arnold and P. Yang. *Angew Chem Int Ed.* 2008, **47**, 6456.
11 K. Kneipp et al. *Spectrochim Acta Part A*, 1995, **51**, 2171.
12 Z. Xu, J. Hao, W. Braida, D. Strickland, F. Li and X. Meng. *Langmuir*, 2011, **27**, 13773.
13 J. F. Li et al. *Nature*, 2010, **464**, 392.
14 C. G. Khoury and T. Vo-Dinh, *J Phys Chem C*, 2008, **112**, 18849.
15 W. Niu, Y. A. A. Chua, W. Zhang, H. Huang and X. Lu. *J Am Chem Soc*, 2015, **137**, 10460.
16 S. He, M. W. C. Kang, F. J. Khan, E. K. M. Tan, M. A. Reyes and J. C. Y. Kah. *J Opt*, 2015, **17**, 114013.
17 A. Childs, E. Vinogradova, F. Ruiz-Zepeda, J. J. Velazquez-Salazar and M. Jose-Yacaman. *J Raman Spectrosc*, 2016, **47**, 651.
18 S. Harmsen et al. *Sci Transl Med,* 2015, **7**, 271ra7.
19 D. V. Voronine et al. *Sci Rep*, **2**, 891.
20 P. P. Patra, R. Chikkaraddy, R. P.N. Tripathi, A. Dasgupta and G. V. P. Kumar. *Nat Commun*, 2014, **5**, 4357.
21 R. Dasari and F. P. Zamborini. *Ana Chem*, 2016, **88**, 675.
22 J. M. Baik, S. J. Lee and M. Moskovits. *Nano Lett*, 2009, **9**, 672.
23 Y. Fang, H. Wei, F. Hao, P. Nordlander and H. Xu. *Nano Lett*, 2009, **9**, 2049.
24 R. Chikkaraddy, D. Singh and G. V. P. Kumar. *Appl Phys Lett*, 2012, **100**, 043108.
25 B. Pettinger, P. Schambach, C. J. Villagómez and Nicola Scott. *Ann Rev Phys Chem*, 2012, **63**, 379.
26 E. Bailo and V. Deckert. *Chem Soc Rev*, 2008, **37**, 921.
27 J. Stadler, T. Schmid and R. Zenobi, *Nano Lett*, 2010, **10**, 4514.
28 S. Dick et al. *Adv Mater*, 2016, **28**, 5705.
29 D. Kurouski, M. Mattei and R. P. Van Duyne. *Nano Lett*, 2015, **15**, 7956.
30 Z. Wang, Z. Tian, D. Han and F. Gu. *Appl Mat & Interf*, 2016, **8**, 5466.
31 Y. Kihara, H. Asami and J.-Y. Kohno. *J Phys Chem B*, 2017, DOI: 10.1021/acs.jpcb.7b01277.
32 S. O. Kucheyev, J. R. Hayes, J. Biener, T. Huser, C. E. Talley and A. V. Hamza *APL*, 2006, **89**, 053102.
33 S. J. Barrow, S. Kasera, M. J. Rowland, J. del Barrio and O. A. Scherman. *Chem Rev*, 2015, **115**, 12320.
34 R. Chikkaraddy, B. de Nijs, F. Benz, S. J. Barrow, O. A. Scherman, E. Rosta, A. Demetriadou, P. Fox, O. Hess and J. J. Baumberg. *Nature*, 2016, **535**, 127.
35 D. O. Sigle, S. Kasera, L. O. Herrmann, A. Palma, B. de Nijs, F. Benz, S. Mahajan, J. J. Baumberg and O. A. Scherman. *J Phys Chem Lett,* 2016, **7**, 704.
36 S. Kasera, L. O. Herrmann, J. D. Barrio, J. J. Baumberg and O. A. Scherman. *Sci Rep*, 2014, **4**, 6785.
37 B. de Nijs, R. W. Bowman, L. O. Herrmann, F. Benz, S. J. Barrow, J. Mertens, D. O. Sigle, R. Chikkaraddy, A. Eiden, A. Ferrari, O. A. Scherman and J. J. Baumberg. *Faraday*

Discuss, 2015, **178**, 185.
38 A. Day, A. P. Arnold, R. J. Blanch, and B. J. Snushall, *Org. Chem*, 2001, **66**, 8094.
39 J. Zhao, H.-J. Kim, J. Oh, S.-Y. Kim, J. W. Lee, S. Sakamoto, K. Yamaguchi, K. Kim, Angew. Chem. 2001, **113**, 4363; Angew. Chem. Int. Ed. 2001, **40**, 4233.
40 R. W. Taylor, T.C. Lee, O. A. Scherman, R. Esteban, J. Aizpurua, F. M. Huang, J. J. Baumberg and S. Mahajan. *ACS Nano*, 2011, **5**, 3878.
41 R. W. Taylor, R. Esteban, S. Mahajan, J. Aizpurua and J. J. Baumberg. *J Phys Chem C*, 2016, **120**, 10512.
42 Kim, J. et al. *J. Am. Chem. Soc.* 2000, **122**, 540.
43 H. Wu, Q. Gong, D. H. Olson and J. Li. *Chem Rev,* 2012, **112**, 836.
44 M. Yuji, A. Kazuaki, I. Takahiko, *Angew Chem,* 2002, **41**, 3020.
45 K. A. Kellersberger, J. D. Anderson, S. M. Ward, K. E. Krakowiak, and D. V. Dearden *J Am Chem Soc*, 2001, **123**, 11316.
46 X.-L. Ni, et al., *Chem Soc Rev,* 2013, **42**, 9480.